Rodent intestinal folate transporters (SLC46A1): secondary structure, functional properties, and response to dietary folate restriction

Andong Qiu,[1,2] Sang Hee Min,[1] Michaela Jansen,[3] Usha Malhotra,[1] Eugenia Tsai,[1,2] Diane C. Cabelof,[4] Larry H. Matherly,[4,5] Rongbao Zhao,[1,2] Myles H. Akabas,[1,3] and I. David Goldman[1,2]

Departments of [1]Medicine, [2]Molecular Pharmacology, and [3]Physiology and Biophysics, Albert Einstein College of Medicine, Bronx, New York; [4]Developmental Therapeutics Program, Barbara Ann Karmanos Cancer Institute, and [5]Department of Pharmacology, Wayne State University School of Medicine, Detroit, Michigan

Qiu A, Min SH, Jansen M, Malhotra U, Tsai E, Cabelof DC, Matherly LH, Zhao R, Akabas MH, Goldman ID. Rodent intestinal folate transporters (SLC46A1): secondary structure, functional properties, and response to dietary folate restriction. *Am J Physiol Cell Physiol* 293: C1669–C1678, 2007. First published September 26, 2007; doi:10.1152/ajpcell.00202.2007.—This laboratory recently identified a human gene that encodes a novel folate transporter [*Homo sapiens* proton-coupled folate transporter (*Hs*PCFT); SLC46A1] required for intestinal folate absorption. This study focused on mouse (*Mus musculus*) PCFT (*Mm*PCFT) and rat (*Rattus norvegicus*) PCFT (*Rn*PCFT) and addresses their secondary structure, specificity, tissue expression, and regulation by dietary folates. Both rodent PCFT proteins traffic to the cell membrane with the NH_2- and COOH-termini accessible to antibodies targeted to these domains only in permeabilized HeLa cells. This, together with computer-based topological analyses, is consistent with a model in which rodent PCFT proteins likely contain 12 transmembrane domains. Transport of [^{3}H]folates was optimal at pH 5.5 and decreased with increasing pH due to an increase in K_m and a decrease in V_{max}. At pH 7.0, folic acid and methotrexate influx was negligible, but there was residual (6*S*)5-methyltetrahydrofolate transport. Uptake of folates in PCFT-injected *Xenopus* oocytes was electrogenic and pH dependent. Folic acid influx K_m values of *Mm*PCFT and *Rn*PCFT, assessed electrophysiologically, were 0.7 and 0.3 μM at pH 5.5 and 1.1 and 0.8 μM at pH 6.5, respectively. Rodent PCFTs were highly specific for monoglutamyl but not polyglutamyl methotrexate. *Mm*PCFT mRNA was highly expressed in the duodenum, proximal jejunum, liver, and kidney with lesser expression in the brain and other tissues. *Mm*PCFT protein was localized to the apical brush-border membrane of the duodenum and proximal jejunum. *Mm*PCFT mRNA levels increased ~13-fold in the proximal small intestine in mice fed a folate-deficient vesus folate-replete diet, consistent with the critical role that PCFT plays in intestinal folate absorption.

intestinal folate absorption; proton-coupled folate transporters; heme carrier protein-1; hereditary folate malabsorption

FOLATES are essential one-carbon donors critical for nucleic acid synthesis and methylation reactions (28). The requirement for this B vitamin is met entirely from the absorption of dietary folates in the proximal small intestine. Recently, this laboratory identified a novel folate transporter [*Homo sapiens* proton-coupled folate transporter (*Hs*PCFT); SLC46A1, GenBank Accession No. NP_542400], which is highly expressed in the human proximal small intestine with functional characteristics similar to what is observed in intestinal folate absorption and transport into cells and membrane vesicles of intestinal origin (22). This transporter was shown to be mutated with a loss of function in the autosomal recessive disorder hereditary folate malabsorption (22, 37). These observations established *Hs*PCFT as essential for intestinal folate absorption and homeostasis in humans (22). Low-pH folate transport activities, with properties similar to those of PCFT, have also been observed in a variety of other normal tissues (liver, kidney, and retina) along with murine and human cancer cell lines (1, 8, 9, 26, 27, 35).

Prior to the identification of *Hs*PCFT, the reduced folate carrier (RFC), an anion exchanger, was often considered to represent the mechanism of intestinal folate absorption because it is highly expressed along the entire intestinal apical brush-border membrane and its expression is increased under conditions of folate deficiency (4, 15, 23). However, RFC-mediated transport has a pH optimum of 7.4 and a specificity profile (very low affinity for folic acid; influx K_i: ~200 μM) that is very different from that observed for folate transport in the intestine and in cells and membrane vesicles of intestinal origin (low pH optimum, high affinity for folic acid; influx K_m: ~0.5 μM) (16, 30). Further evidence that the intestinal folate absorptive process is genetically distinct from RFC came from studies in which the low-pH folate transport activity was preserved in cell lines of intestinal and other tissue origins even when RFC was deleted from the genome or mutated with a loss of function (3, 29, 35, 36).

The present study addresses the functional properties and secondary structure of PCFT orthologs in the mouse [*Mus musculus* (*Mm*)PCFT] and rat [*Rattus norvegicus* (*Rn*)PCFT] along with the tissue expression pattern, specificity, and regulation in mice in response to dietary folate restriction. These experiments provide fundamental information necessary for the further characterization of the role of PCFT in mouse development and folate delivery to intestinal and other tissues and for the investigation of PCFT as a factor in the pathogenesis of cancer in mouse models.

MATERIALS AND METHODS

Reagents. [^{3}H]folic acid, [^{3}H]methotrexate (MTX), and [^{3}H](6*S*)5-methyltetrahydrofolate (5-methylTHF) were obtained from Moravek Biochemicals (Brea, CA) and purified as previously described (5). MTX di-, tri-, tetra-, penta-, and hexaglutamates, (6*S*)5-methylTHF, and (6*S*)- and (6*R*)5-formyltetrahydrofolate (5-formylTHF) were ob-

tained from Schircks Laboratories (Jona, Switzerland). PT523, a MTX analog, was obtained from Andre Rosowsky (Dana Farber Cancer Institute, Boston, MA). Folic acid, MTX, and other chemicals were obtained from commercial sources.

Plasmid construction. Full-length *Mm*PCFT and *Rn*PCFT cDNA clones were obtained from Open Biosystems (Huntsville, AL). The open reading frames (ORFs) were PCR amplified with PfuUltra DNA polymerase (primers are shown in Table 1) and subsequently cloned into the *Bgl*II site of the pS64T vector for in vitro transcription of the capped sense *Mm*PCFT and *Rn*PCFT cRNA from a SP6 promoter using the mMESSAGE mMACHINE system (Ambion, Austin, TX) and into the *Bam*HI site of pcDNA3.1(+) to generate pcDNA3.1(+)*Mm*PCFT and pcDNA3.1(+)*Rn*PCFT, respectively. *Mm*PCFT and *Rn*PCFT ORFs were tagged at either NH$_2$- or COOH-termini with a hemaglutinin (HA) epitope by PCR (primers shown in Table 1) and cloned into pcDNA3.1(+) with the same strategy as above. cDNA inserts were verified by DNA sequencing at the Albert Einstein Cancer Center Genomics Shared Resource.

Cell culture and transfection. HeLa and HepG2 cells obtained from the American Type Culture Collection (Manassas, VA) were maintained as previously described (30). Plasmid DNA was transfected into these cells using Lipofectamine 2000 (Invitrogen). HepG2 cells stably transfected with either pcDNA3.1(+), pcDNA3.1(+)*Mm*PCFT, or pcDNA3.1(+)*Rn*PCFT were generated by G418 selection (600 µg/ml).

Experiments in mice. The impact of dietary folate restriction on PCFT mRNA levels was assessed in 3- to 4-mo-old male C57BL/6 specific pathogen-free mice. Animals were maintained on either folate-containing mouse chow (2 mg/kg folic acid) or a folic acid-free diet over 8 wk, after which they were killed in a CO$_2$ chamber. The proximal small intestine was dissected and rinsed in ice-cold PBS (pH 7.4), and total RNA was isolated with TRIzol reagent (Invitrogen). Data on RFC and folate receptor (FR)-α levels in these animals have been previously reported (15).

For immunohistochemical experiments, C57BL/6 adult mice maintained on the usual mouse chow were killed, and segments of intestines were dissected, rinsed in ice-cold PBS (pH 7.4), and embedded in freezing embedding OCT medium (Andwin Scientific, Addison, IL) for cryosectioning at 5 µm thickness. Similar intestine segments were dissected for the isolation of total RNA.

Production of peptide antibody and immunohistochemistry. Antiserum specific for *Mm*PCFT protein was custom made by Open

Biosystems in rabbits using the peptide corresponding to amino acids 446–459 ([C]EKVNPHPEFQQFPQSP) of *Mm*PCFT protein as the antigen. Antibodies specific for *Mm*PCFT were affinity purified with the Sulfolink Trial Kit (Pierce). Rabbit anti-HA antibody was obtained from Sigma-Aldrich. Immunofluorescence was performed using either affinity-purified anti-*Mm*PCFT or anti-HA antibodies and secondary swine anti-rabbit IgG antibody conjugated with FITC (DAKO, Carpinteria, CA). HeLa cells were stained with or without permeabilization in 0.2% Triton X-100 in PBS (pH 7.4) for 15 min, and fluorescence was visualized on an Olympus IX70 Inverted Epifluorescence Microscope (Center Valley, PA).

Preparation of cryosections of mouse tissues and immunochemistry with affinity-purified anti-*Mm*PCFT antibody followed procedures previously described (31). The specificity of the anti-*Mm*PCFT antibody was confirmed by blocking the immunohistochemical staining of*Mm*PCFT with the peptide antigen (200 µg/ml).

SDS-PAGE and Western blot analysis. HepG2 or HeLa cell membrane fractions were prepared using previously reported procedures (22). Protein samples (30 µg) were resolved by SDS-PAGE, and *Mm*PCFT protein was detected by Western blot analysis using rabbit anti-*Mm*PCFT peptide antibody solution (1:1,000 dilution) together with goat anti-rabbit horseradish peroxidase-conjugated IgG (1:5,000 dilution, Cell Signaling Technology, Danvers, MA).

Measurement of uptake of folates in HepG2 and HeLa cells. Uptake of [^{3}H]folic acid, [^{3}H]MTX, or [^{3}H](6S)5-methylTHF was assessed in HepG2 and HeLa cells grown in monolayer cultures at the bottom of liquid scintillation vials by modification of previously described procedures (22, 24). Initial uptake kinetics for tritiated folates were measured over a 2-min interval. This resulted in a small (~30%) decrease in extracellular folate, due to cellular uptake, at the lowest concentration studied (0.1 µM). This decreased as the extracellular folate level increased and became negligible at concentrations >1.0 µM. This resulted in a small overestimation of K_m; this would not be a factor in influx kinetic measurements obtained electrophysiologically.

To assess the effects of antiserum on folic acid uptake mediated by *Mm*PCFT, stably transfected HepG2 cells were washed twice in HBS [20 mM HEPES, 140 mM NaCl, 5 mM KCl, 2 mM MgCl$_2$, and 5 mM dextrose (pH 7.4)] and then incubated with 1 ml of HBS (pH 7.4) containing preimmune or anti-*Mm*PCFT serum (1:50 dilution) at 37°C and pH 7.4 for 20 min. [^{3}H]folic acid (0.5 µM) influx was then measured in MBS (20 mM MES, 140 mM NaCl, 5 mM KCl, 2 mM

Table 1. *Primer sequences of MmPCFT and RnPCFT ORFs as well as MmPCFT and GAPDH primers used for quantitative RT-PCR*

	Primer Sequence
*Mm*PCFT ORF	
Forward	5′-TAT<u>AGATCT</u>CACCATGGAGGGGCGCGTGAG-3′
Reverse	5′-TAT<u>AGATCT</u>TCAGGGGCTCTGAGGAAAC-3′
Forward (N-HA tag)	5′-TAT<u>AGATCT</u>CACCATGTACCCATACGATGTTCCAGATTACGCTATGGAGGGGCGCGTGAG-3′
Reverse(C-HA tag)	5′-TCA<u>AGATCT</u>TAAGCGTAATCTGGAACATCGTATGGGTAGGGGCTCTGAGGAAACTG-3′
*Rn*PCFT ORF	
Forward	5′-TCA<u>AGATCT</u>CACCATGGAGGGGCGCGTGAGC-3′
Reverse	5′-TCA<u>AGATCT</u>CAGGAGTTCTGAGGAAACTG-3′
Forward(N-HA tag)	5′-TCA<u>AGATCT</u>CACCATGTACCCATACGATGTTCCAATTACGCTATGGAGGGGCGCGTGAGC-3′
Reverse(C-HA tag)	5′-TCA<u>AGATCT</u>TAAGCGTAATCTGGAACATCGTATGGGTAGGAGTTCTGAGGAAACTG-3′
Quantitative RT-PCR	
*Mm*PCFT	
Forward	5′-GAATGGTGGTCTTTGCGTTT-3′
Reverse	5′-TCCGTACCCTGTGAACATGA-3′
GAPDH	
Forward	5′-GGCATTGCTCTCAATGACAA-3′
Reverse	5′-CCCTGTTGCTGTAGCCGTAT-3′

*Mm*PCFT, mouse (*Mus musculus*) protein-coupled folate transporter (PCFT); *Rn*PCFT, rat (*Rattus norvegicus*) PCFT; ORF, open reading frame; N-HA and C-HA tags, NH$_2$- and COOH-terminal hemaglutin tags, respectively. Underlined regions indicate *Bgl*II restriction sites.

MgCl$_2$, and 5 mM dextrose) at pH 5.5 or 6.5 containing either preimmune or anti-*Mm*PCFT serum (1:50 dilution) at 37°C for 2 min.

To examine the effects of sodium on the transport activities of *Mm*PCFT or *Rn*PCFT, [^{3}H]folic acid (0.5 μM) uptake was assessed in MBS (pH5.5) over 2 min in which 140 mM NaCl was replaced by the same concentration of choline chloride. Uptake was normalized to protein content.

Electrophysiological analyses in Xenopus oocytes. Preparation and microinjection with 50 nl of water or PCFT cRNA (30–50 ng) into defolliculated *Xenopus laevis* oocytes followed previously described procedures; oocytes were kept at 17°C in horse serum medium [82.5 mM NaCl, 2.5 mM KCl, 1 mM MgCl$_2$, 2.3 mM CaCl$_2$, 5 mM HEPES, and 5% horse serum (pH 7.5)], and electrophysiological recordings in a solution of 90 mM NaCl, 1 mM KCl, 1 mM MgCl$_2$, 1.8 mM CaCl$_2$, 5 mM Tris, and 5 mM MES were conducted 3–7 days after cRNA injection (10, 22). For the determination of K_m values, currents were measured at different folate concentrations with the membrane potential clamped at −80 mV. Influx kinetic constants were obtained from the normalized currents from different experiments fitted to the following equation: $I = (I_{max} \times S)/(K_m + S)$, where I is the current induced by a given substrate concentration (S) and I_{max} is the maximal current generated.

Northern blot analysis. A Northern blot containing polyA$^+$ RNA (2 μg/lane) from 12 mouse tissues was obtained from Origene (Rockville, MD). [^{32}P]dCTP-labeled cDNA probes were made from a *Mm*PCFT cDNA segment (1094–1440 bp, GenBank Accession No. NM_026740) and hybridized to the membrane as previously described (22). After the membrane had been stripped, β-actin mRNA was probed as the loading control.

Total RNA (10 μg) isolated from different intestinal segments was resolved on a 1% denaturing agarose gel and transferred to a Nytran nylon membrane (Whatman, Florham Park, NJ). Northern blot hybridization was subsequently performed using the [^{32}P]dCTP-labeled *Mm*PCFT cDNA probe described above. 18S and 28S rRNAs were visualized after ethidium bromide staining as the loading control.

Quantitative RT-PCR. Total RNA isolated from mice fed folate-replete or folate-deficient diets, as previously reported (15) and described above, was reverse transcribed to cDNA with Superscript Reverse Transcriptase II (Invitrogen). Real-time PCR was performed with SYBR Green PCR Master Mix (Applied Biosystems, Foster City, CA) and primers specific for *Mm*PCFT (Table 1). GAPDH was simultaneously amplified with specific primers (Table 1) to normalize *Mm*PCFT expression.

RESULTS

*Structural analysis of MmPCFT and RnPCFT. Mm*PCFT and *Rn*PCFT (GenBank Accession Nos. AAH57976 and AAH89868, respectively) were identified in the National Center for Biotechnology Information (NCBI) GenBank database based on high amino acid identity to human PCFT protein. The human, mouse, and rat orthologs encode proteins of 459 amino acids with a predicted molecular weight of ∼50 kDa (Fig. 1*A*). PCFT proteins are highly conserved in mammals. Based on sequence alignment analysis with ClustalW (13), the predicted *Mm*PCFT and *Rn*PCFT proteins share 95% amino acid identity to each other, 87% identity to *Hs*PCFT, and >80% identity to their counterparts in other mammalian species, e.g., the dog (*Canis familiaris*; XP_548286), rhesus monkey (*Macaca mulatta*; XP_001106954), and domestic cow (*Bos taurus*; XM_588367) (Fig. 1, *A* and *B*). PCFT orthologs also appear to be present in nonmammalian vertebrates, e.g., the chicken [*Gallus gallus* (*Gg*PCFT); XP415815], African clawed frog [*X. laevis* (*Xl*PCFT); AAH77859], and zebrafish [*Danio rerio* (*Dr*PCFT); AAH49421], all of which share >50% amino acid

identity to mammalian PCFTs (Fig. 1*B*). No invertebrate homologs could be identified in the NCBI GenBank database with >30% amino acid identity to vertebrate PCFTs.

*Mm*PCFT and *Rn*PCFT genes are located at Chr11B5 and Chr10q25, respectively, and have the same gene structure as *Hs*PCFT (Chr17q11.2): five exons and four introns with exons highly conserved between these three species (Fig. 1*C*). Similar gene structure and exon conservation are also present in other *PCFT* genes, for instance, the dog (GeneID: 491166), rhesus monkey (GeneID: 708727), domestic cow (GeneID: 511097), and chicken (GeneID: 417569). The zebrafish (GeneID: 393255) gene contains six exons and five introns; exons 2 and 3 of the *DrPCFT* gene correspond to exon 2 of the mammalian and chicken *PCFT* genes.

Subcellular localization and topological properties of MmPCFT and RnPCFT proteins. Topology prediction programs [DAS, HMMTOP, PredictProtein, SOSUI, TMHMM, TMpred, TopPred, and Hydropathy Analysis (http://www.expasy.org/tools/#topology and http://www.tcdb.org/analyze.php)] were employed to characterize the PCFT secondary structure. The numbers of transmembrane domains (TMDs) varied with the different algorithms. Most of the programs predicted a polytopic integral membrane protein with 11 or 12 transmembrane segments, although TMpred predicted 10 transmembrane segments. A model with 12 TMDs, as predicted by DAS, HMMTOP, ProteinPrediction, and Hydropathy Analysis programs, is shown in Fig. 1*A* and indicates the high degree of homology within TMDs among human and rodent transporters.

An immunohistochemistry approach was used to assess the location of the NH$_2$- and COOH-termini of rodent PCFT proteins. *Mm*PCFT and *Rn*PCFT were tagged with an HA epitope at either terminus, and the fusion proteins were subsequently immunodetected with an anti-HA antibody in HeLa cells transiently transfected with each construct with or without permeabilization before being immunostained. As shown in Fig. 2*A*, *Mm*PCFT and *Rn*PCFT HA fusion proteins could only be localized to the plasma membrane of permeabilized cells (*top*); these epitopes could not be stained in cells that were not permeabilized (*bottom*). Similar immunolocalization was also observed for wild-type *Mm*PCFT expressed in HeLa cells (Fig. 2*A*, wild-type *Mm*PCT), which could only be stained in permeabilized cells with an anti-*Mm*PCFT peptide antibody that specifically recognizes an epitope in the COOH-terminus. These observations are consistent with an intracellular localization of the NH$_2$- and COOH-termini of *Mm*PCFT and *Rn*PCFT and a predicted topology in which there are an even number of transmembrane segments, likely 12 transmembrane segments, as based on the topological analyses.

When cDNAs encoding wild-type or HA-tagged transporters were transiently transfected into HeLa cells, all the constructs noted above produced [^{3}H]MTX influx activity comparable with that of cells transfected with native *Mm*PCFT and *Rn*PCFT, which was >14 times higher than cells transfected with vector control alone (Fig. 2*B*, mock) and consistent with their plasma membrane localization and the reported folate transport activity for the human gene (22). This also indicates that the HA epitope at either the NH$_2$- or COOH-terminus does not alter the transport activity of *Mm*PCFT or *Rn*PCFT.

Anti-*Mm*PCFT serum, which specifically recognizes the COOH-terminus of the murine transporter, did not alter folic acid uptake in HepG2 cells stably transfected with *Mm*PCFT,
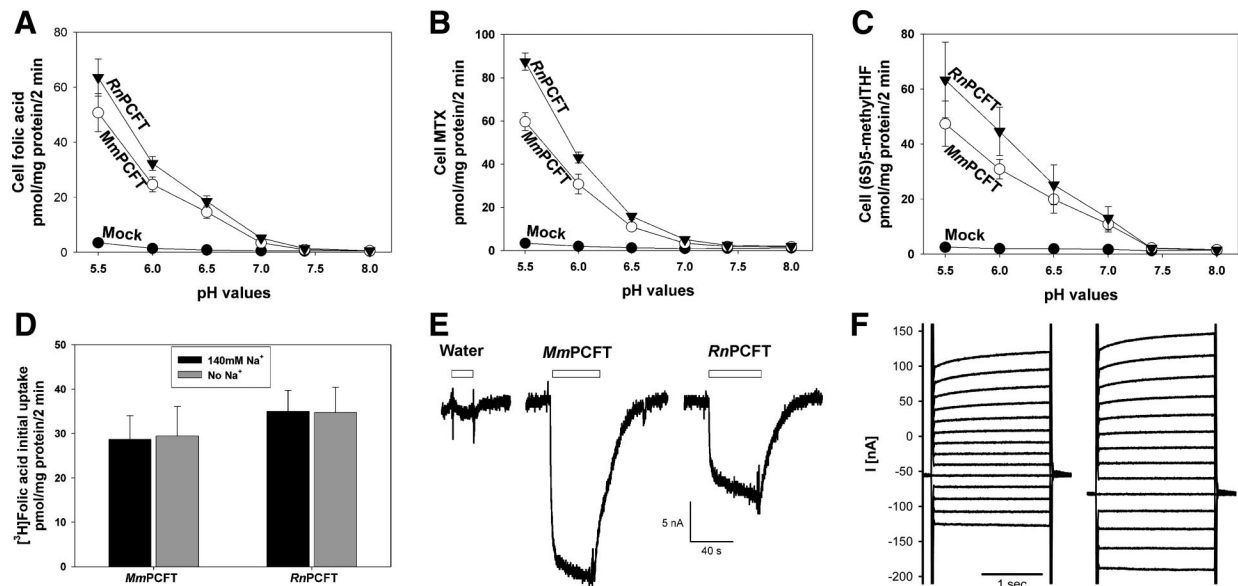
A

```
MmPCFT   1 MEGRVSSVGSPHSFLNAPVLFRGPVEPLVFLANFALVLQGPLTTQYLWHRFSTELGYNGTRHRENCGNQSADPLMKEVET 80
RnPCFT   1 MEGRVSPVGSSHRLLTAAVLFRGPVEPLVFLANFALVLQGPLTTQYIWHRTSTELGYNGTRHRENCGNQSADPVLKEVET 80
HsPCFT   1 MEGSASPPEKPRARPAAAVLCRGPVEPLVFLANFALVLQGPLTTQYLWHRFSADLGYNGTRQRGGCSNRSADPTMQEVET 80
                                          TMD 1
MmPCFT  81 LTSHWTLYMNVGGFLVGLFWSTLLGAWSDRVGRRPLLVLASLGLLLQAVVSIFVVQLELHVGFFVLGRALCALLGDFNGL 160
RnPCFT  81 LTSHWTLYMNVGGFLVGLFWSTLLGAWSDRVGRRPLLVLASLGLLLQAVVSIFVVQLQLHIGFFVLGRALCALLGDFNGL 160
HsPCFT  81 LTSHWTLYMNVGGFLVGLFSSTLLGAWSDSVGRRPLLVLASLGLLLQALVSVFVVQLQLHVGYFVLGRILCALLGDFGGL 160
                TMD 2                           TMD 3                              TMD 4
MmPCFT 161 LAASFASVADVSSNHSRTFRMALLEACIGVAGTLASLLGGHWLRAQGYANPFWLALALLIVMALYAAFCFGETVKEPKST 240
RnPCFT 161 LAASFASVADVSSNHSRTFRMALLEACIGVAGTLASLLGGHWLRAQGYANPFWLALAVLIVMTLYAAFCFGETVKEPKST 240
HsPCFT 161 LAASFASVADVSSSRSRTFRMALLEASIGVAGMLASLLGGHWLRAQGYANPFWLALALLIAMTLYAAFCFGETLKEPKST 240
                              TMD 5                           TMD 6
MmPCFT 241 RLFTLRHHRSIARLYVVPAPEKSRMHLALYSLAIFVVVTVHFGAQDILTLYELSAPLCWDSKLIGYGSAAQHLPYLTSLL 320
RnPCFT 241 RLFTLRHHRSIVQLYVVPAPEKSRMHLALYSLAIFVVVTVHFGAQDILTLYELSTPLCWDSKLIGYGSAAQHLPYLTSLL 320
HsPCFT 241 RLFTFRHHRSIVQLYVAPAPEKSRKHLALYSLAIFVVITVHFGAQDILTLYELSTPLCWDSKLIGYGSAAQHLPYLTSLL 320
                              TMD 7                           TMD 8
MmPCFT 321 GLRLLQFCLADTWVAEIGLAFNILGMVVFAFATITPLMFTGYGLLFLSLVTTPVIRAKLSKLVSESEQGALFSAVACVNS 400
RnPCFT 321 GLRLLQFCLADTWVAEIGLAFNILGMVVFAFATITPLMFTGYGLLFLSLVTTPVIRAKLSKLVSESEQGALFSAVACVNS 400
HsPCFT 321 ALKLLQYCLADAWVAEIGLAFNILGMVVFAFATITPLMFTGYGLLFLSLVITTPVIRAKLSKLVRETEQGALFSAVACVNS 400
                TMD 9                           TMD 10
MmPCFT 401 LAMLMASGIFNSIYPATLNFMKGFPFLLGAGLLFIPAILIGVLEKVNPHPEFQQFPQSP 459
RnPCFT 401 LAMLMASGIFNSLYPATLNFMKGFPFLLGAGLLFIPAILIGVLEKVNPHPEFQQFPQNS 459
HsPCFT 401 LAMLTASGIFNSLYPATLNFMKGFPFLLGAGLLLIPAVLIGMLEKADPHLEFQQFPQSP 459
       TMD 11                     TMD 12
```

B

	HsPCFT	MmPCFT	RnPCFT	GgPCFT	XlPCFT
DrPCFT	52	53	52	57	63
XlPCFT	57	57	56	61	
GgPCFT	55	55	54		
RnPCFT	87	95			
MmPCFT	87				

C

Fig. 1. Homology comparison of proton-couple folate transporters (PCFTs) among vertebrates. *A*: amino acid sequence alignment of mouse (*Mus musculus*) PCFT (*Mm*PCFT), rat (*Rattus norvegicus*) PCFT (*Rn*PCFT), and human (*Homo sapiens*) PCFT (*Hs*PCFT). Shaded residues represent positions of identity or similarity among these sequences. The 12 transmembrane domains (TMDs) predicted by DAS, HMMTOP, ProteinPrediction, and Hydropathy Analysis (http://www.expasy.org/tools/#topology; http://www.tcdb.org/analyze.php) are underlined and numbered as *1–12*. The potential *N*-glycosylation sites between *TMD 1* and *TMD 2* are underlined in gray. Residues in black with white letters indicate identity and residues in gray with white letters indicate similarity among the species. *B*: amino acid sequence identity, expressed as percentages, among vertebrate PCFT proteins based on whole protein alignment with ClustalW (http://www.ebi.ac.uk/clustalw/index.html). *Gg*PCFT, *Gallus gallus* PCFT; *Xl*PCFT, *Xenopus laevis* PCFT; *Dr*PCFT, *Danio rerio* PCFT. *C*: comparison of gene structure, mRNA, and predicted TMDs of *Mm*PCFT and *Hs*PCFT.

further supporting the intracellular localization of the COOH-terminus of *Mm*PCFT protein (Fig. 2*C*).

Using anti-*Mm*PCFT serum, *Mm*PCFT protein was detected as broad bands in the Western blot analysis in both transiently transfected HeLa cells and stably transfected HepG2 cells with molecular weights higher than predicted (~50 kDa) (Fig. 2*D*). This is consistent with the *N*-linked glycosylation site(s) in the extracellular loop between *TMD 1* and *TMD 2*, which are

Fig. 2. Cellular localization and functional expression of *Mm*PCFT and *Rn*PCFT in HeLa and HepG2 cells. *A*: cellular localization of wild-type *Mm*PCFT, *Mm*PCFT/C-HA, *Rn*PCFT/C-HA, *Mm*PCFT/N-HA, and *Rn*PCFT/N-HA proteins expressed in HeLa cells with (*top*) or without (*bottom*) prior membrane permeabilization with 0.2% Triton X-100 in PBS for 15 min. Wild-type *Mm*PCFT protein was detected with an affinity-purified polyclonal peptide antibody that recognizes the COOH-terminus, whereas hemaglutinin (HA)-tagged PCFT proteins were detected with a commercial anti-HA antibody. C-HA and N-HA indicate tagged PCFTs with a HA epitope at the COOH- or NH$_2$-termini, respectively. Images shown are representative of 3–4 independent immunostainings. *B*: initial uptake of 0.5 μM [^{3}H]methotrexate (MTX) at pH 5.5 and 37°C for 2 min in HeLa cells transiently transfected with pcDNA3.1(+) (mock), pcDNA3.1(+) *Mm*PCFT, pcDNA3.1(+) *Rn*PCFT, pcDNA3.1(+) *Mm*PCFT/C-HA, pcDNA3.1(+) *Rn*PCFT/C-HA, pcDNA3.1(+) *Mm*PCFT/N-HA, and pcDNA3.1(+) *Rn*PCFT/N-HA. Data are means ± SE from 3 independent experiments. *C*: mock-transfected or *Mm*PCFT stably transfected HepG2 cells were incubated in HBS with preimmune serum or anti-*Mm*PCFT serum (1:50 dilution) at pH 7.4 and 37°C for 20 min, after which influx of 0.5 μM [^{3}H]folic acid was assessed at pH 5.5 and 37°C over 2 min in uptake buffer containing the same concentrations of preimmune serum or anti-*Mm*PCFT serum. Data are means ± SE from 3 independent experiments. *D*: Western blot of *Mm*PCFT in transiently transfected HeLa cells and stably transfected HepG2 cells.

highly conserved among rodent and human PCFTs (Fig. 1*A*) and have been confirmed in other studies by this laboratory (unpublished observations). In both HepG2 and HeLa transfectants, there was a band at ~35 kDa detected in both mock- and *Mm*PCFT-transfected HeLa and HepG2 cells that disappeared in the presence of blocking peptide. The origin of this band was not clear.

pH dependence of folate transport mediated by MmPCFT and RnPCFT. The initial uptake of 0.5 μM [^{3}H]folic acid (Fig. 3*A*), [^{3}H]MTX (Fig. 3*B*), and [^{3}H](6*S*)5-methylTHF (Fig. 3*C*) by *Mm*PCFT and *Rn*PCFT in stably transfected HepG2 cells was highly pH dependent, decreasing as pH was increased from pH 5.5 to 7.4. Whereas there was negligible folic acid and MTX transport at pH 7.0, there was residual activity for (6*S*)5-methylTHF at this pH. There was ~50% of maximum activity for all these folate substrates at pH 6.0, the pH at the upper small intestinal absorptive surface (17). [^{3}H]folic acid

transport mediated by *Mm*PCFT and *Rn*PCFT in stably transfected HepG2 cells was not sodium dependent; influx of both species was the same in sodium-containing buffer and buffer in which sodium was replaced by choline (Fig. 3*D*).

Electrophysiological characterization of MmPCFT and RnPCFT in Xenopus oocytes. Xenopus oocytes injected with either *Mm*PCFT or *Rn*PCFT cRNA displayed currents induced by folic acid, (6*S*)5-methylTHF, or MTX in two-electrode voltage-clamp experiments (shown for folic acid in Fig. 3*E*); no currents were induced by folates in water-injected oocytes. In general, the folate-induced current amplitude was greater with *Mm*PCFT than with *Rn*PCFT. Folic acid-induced current amplitudes were proportional to the applied transmembrane voltage in oocytes expressing either *Mm*PCFT (Fig. 3*F*) or *Rn*PCFT (data not shown).

Folate influx kinetics. Initial rates of [^{3}H]folic acid, [^{3}H]MTX, and [^{3}H](6*S*)5-methylTHF uptake in HepG2 cells stably trans-

Fig. 3. pH dependence of folate transport mediated by MmPCFT and RnPCFT and electrophysiological analyses in *Xenopus* oocytes. *A–C*: initial uptake rates of 0.5 µM [^{3}H]folic acid (*A*), [^{3}H]MTX (*B*), or [^{3}H](6S)5-methyltetrahydrofolate (5-methylTHF; *C*) were assayed in mock-, MmPCFT-, and RnPCFT-transfected HepG2 cells as a function of pH at 37°C over 2 min. *D*: initial rates of 0.5 µM [^{3}H]folic acid uptake were assessed in mock-, MmPCFT-, and RnPCFT-transfected HepG2 cells in control MES buffer containing 140 mM NaCl or sodium-free MES buffer at pH5.5 and 37°C over 2 min. Data in *A–D* are means ± SEM from 3–4 independent experiments. *E*: currents elicited by application of 16.5, 16.5, and 6.8 µM folic acid (16.5 and 6.8 µM are equal to 25× the electrophysiologically determined K_m at pH 5.5 for MmPCFT and RnPCFT, respectively) to voltage-clamped *Xenopus* oocytes injected with water, MmPCFT, or RnPCFT cRNA, respectively. The holding potential (V_h) was −80 mV; bath pH was 5.5. Open boxes above the current traces indicate the intervals of folic acid application. *F*: membrane currents (*I*) from an oocyte expressing MmPCFT (*left*, perfused with buffer at pH 5.5; *right*, perfused with folic acid at a concentration 25× K_m at pH 5.5). Responses to depolarizing and hyperpolarizing voltage clamp steps are shown. Oocytes were held at a V_h of −60 mV, and the voltage was stepped for 2 s in 10-mV increments from −100 to +30 mV.

fected with cDNAs encoding MmPCFT and RnPCFT followed Michaelis-Menten kinetics (as illustrated for folic acid in Fig. 4*A*). Folic acid-induced currents in *Xenopus* oocytes injected with MmPCFT cRNA was saturable with increasing substrate concentrations at both pH 5.5 and 6.5 (Fig. 4*B*). Table 2

shows data comparing relative influx K_m values for the various folates for mouse and rat PCFTs at pH 5.5 versus 6.5. Both MmPCFT and RnPCFT had comparable high affinities for folic acid at pH 5.5. When pH was increased from 5.5 to 6.5, the K_m value for folic acid, (6S)5-methylTHF, and MTX was in-

Fig. 4. Influx kinetics and substrate specificity of MmPCFT and RnPCFT. *A*: initial uptake of [^{3}H]folic acid as a function of substrate concentrations at pH 5.5. *B*: electrophysiological analysis of folic acid-induced currents as a function of concentration in *Xenopus* oocytes expressing MmPCFT (pH 5.5, V_h = −80 mV). Currents were normalized to the maximum current (I_{max}) for each oocyte. Each data point is the average of at least 3 oocytes from at least 2 different batches of oocytes. Data are presented as means ± SE. *C*: influx of 0.5 µM [^{3}H]folic acid was assessed at pH 5.5 and 37°C over 2 min in the absence (control) or presence of 5 µM of nonlabeled folates or antifolates in MmPCFT- and RnPCFT-transfected HepG2 cells. Differences between experimental groups were analyzed using nonparametric ANOVA followed by Tukey's test. *D*: influx of 0.5 µM [^{3}H]MTX was assayed as described above in the absence (control) or presence of 50 µM nonlabeled MTX or MTX diglutamate (MTX-Glu1), triglutamate (MTX-Glu2), tetraglutamate (MTX-Glu3), pentaglutamate (MTX-Glu4), or hexaglutamate (MTX-Glu5). Data in *A*, *C*, and *D* are means ± SE from 3–4 independent experiments.
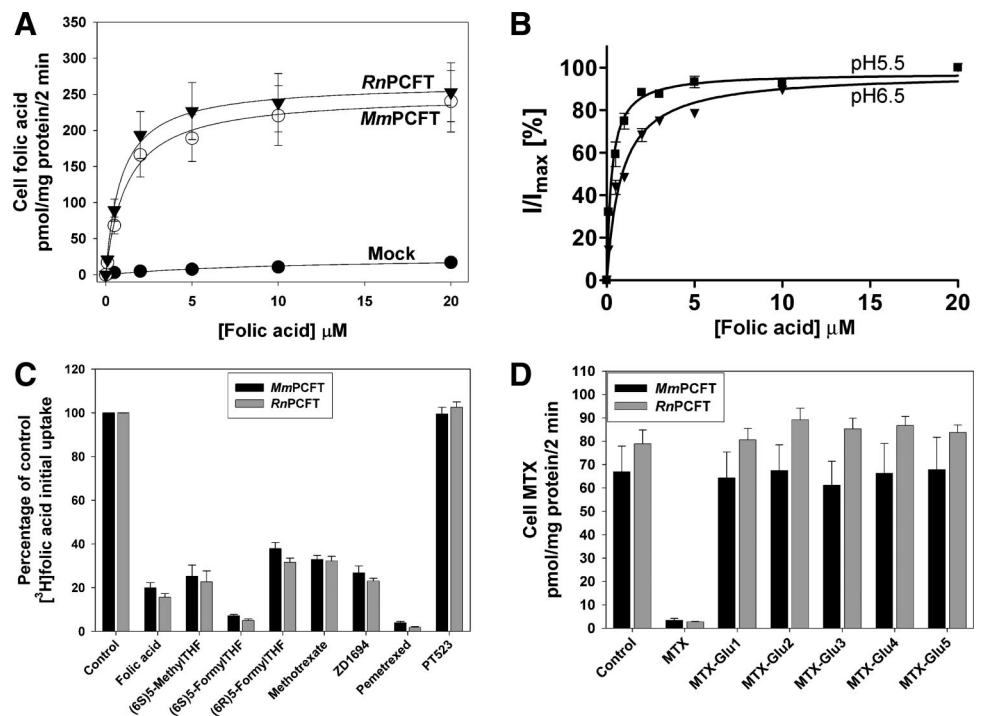
Table 2. *Relative influx K_m values for the various folates for MmPCFT and RnPCFT at pH 5.5 versus 6.5*

	pH 5.5	pH 6.5
Influx measurements with tritiated folates		
Folic acid		
*Mm*PCFT	1.1±0.1	3.9±0.4
*Rn*PCFT	0.8±0.1	2.1±0.4
(6S)5-methylTHF		
*Mm*PCFT	0.8±0.2	1.6±0.8
*Rn*PCFT	0.7±0.1	1.3±0.4
MTX		
*Mm*PCFT	1.0±0.1	4.6±1.8
*Rn*PCFT	0.6±0.1	2.6±0.8
Electrophysiological measurements		
Folic acid		
*Mm*PCFT	0.7±0.1	1.1±0.1
*Rn*PCFT	0.3±0.0	0.8±0.0
(6S)5-MethylTHF		
*Mm*PCFT	0.3±0.0	0.3±0.0

Data are means ± SE of K_m values (in μM). The following substrates were used: folic acid, (6S)5-methyltetrahydrofolate {(6S)5-methylTHF}, and methotrexate (MTX).

creased and V_{max} was decreased. For instance, K_m values for MTX increased from 1.0 ± 0.1 and 0.6 ± 0.1 μM to 4.6 ± 1.8 and 2.6 ± 0.8 μM for *Mm*PCFT and *Rn*PCFT, respectively, and V_{max} decreased from 289.6 ± 48.8 and 281.3 ± 32.8

pmol·mg protein^{-1}·2 min^{-1} to 137.9 ± 24.2 and 130.2 ± 16.1 pmol·mg protein^{-1}·2 min^{-1}, respectively. There was a lesser change in influx K_m values for folic acid over this pH range, with no change for (6S)5-methylTHF as assessed by electrophysiological measurements in *Xenopus* oocytes (Table 2). K_m values were somewhat overestimated using tritiated folates due to substrate depletion at low concentrations, which could account for differences in this parameter based on current measurements (see MATERIALS AND METHODS). In addition, these differences might be due to voltage-related changes in K_m that occur during electrophysiological measurements.

MmPCFT and RnPCFT substrate specificity. Influx of 0.5 μM [³H]folic acid was assessed at pH 5.5 in the absence (control) or presence of a 10-fold (5 μM) higher concentration of nonlabeled folates or antifolates in *Mm*PCFT-, *Rn*PCFT-, and mock-transfected HepG2 cells. As shown in Fig. 4*C*, there was substantial inhibition of [³H]folic acid uptake by folates and antifolates. The most potent inhibitors were pemetrexed and (6S)5-formylTHF followed by folic acid and (6S)5-methylTHF and then MTX and ZD1694 ($P < 0.001$). The unnatural (6R) isomer of 5-formylTHF was a weaker inhibitor than the natural (6S) isomer ($P < 0.001$, as assessed by one-way ANOVA followed by Tukey's test). PT523, a 4-amino folic acid (aminopterin) analog with a hemiphthaloyl-L-ornithine side chain, did not inhibit at all.

As shown in Fig. 4*D*, whereas uptake of 0.5 μM [³H]MTX at pH 5.5 mediated by *Mm*PCFT and *Rn*PCFT was nearly
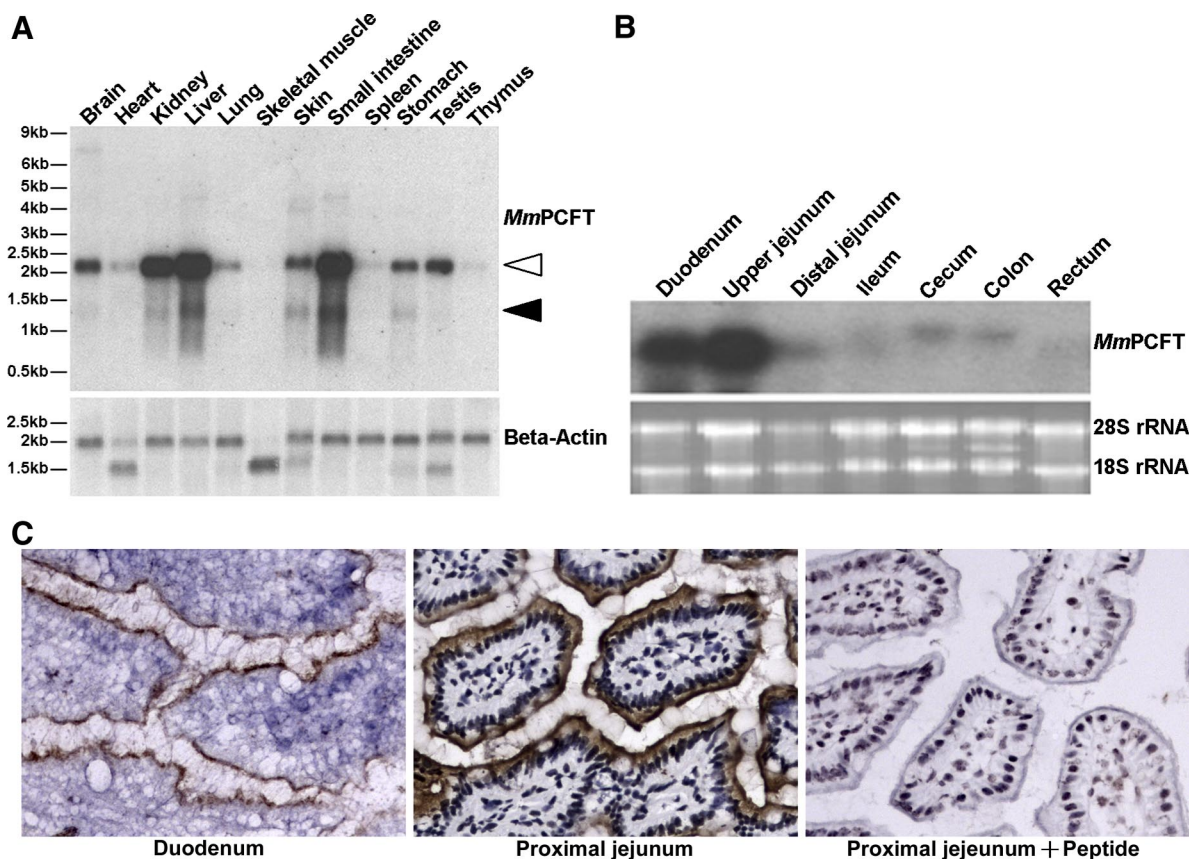
Fig. 5. *Mm*PCFT mRNA and protein levels in mouse tissues. *A*: *Mm*PCFT mRNA levels in mouse tissues by Northern blot analysis. β-Actin was probed as a loading control. Open and filled arrowheads indicate the location of major and minor *Mm*PCFT mRNA transcripts, respectively. *B*: *Mm*PCFT mRNA levels in the mouse intestine. Data are representative of 2 mice. *C*: expression and localization of *Mm*PCFT protein in the mouse duodenum (*left*) and proximal jejunum (*middle*). The peptide used to produce the anti-*Mm*PCFT antibody neutralized anti-*Mm*PCFT antibody activities in control staining (*right*), indicating the high specificity of this antibody.

abolished by 50 μM nonlabeled MTX monoglutamate, the same concentration of MTX di-, tri-, tetra-, penta-, or hexaglutamate had no inhibitory effect at all, indicating that *Mm*PCFT and *Rn*PCFT are highly specific for monoglutamyl forms of folates.

Expression of PCFT mRNA and protein in mouse tissues. *Mm*PCFT mRNA, with a molecular size of ∼2.2 kb, was abundantly expressed in the small intestine, liver, and kidney and to a lesser extent in the brain, testis, skin, and stomach (Fig. 5A). There were low levels in the heart and lung, very low levels in the spleen and thymus, and no detectable *Mm*PCFT mRNA in skeletal muscle. A shorter isoform of *Mm*PCFT mRNA, with a molecular size of ∼1.3 kb, was also detected in the brain, kidney, liver, skin, small intestine, and stomach. Focusing on the intestinal tract, *Mm*PCFT mRNA was highly expressed in the duodenum and proximal jejunum, with lower expression in the distal jejunum and even lower levels in the cecum and colon (Fig. 5B). There was just a trace of expression in the ileum and rectum.

*Mm*PCFT protein localization was analyzed by immunohistochemistry using affinity-purified polyclonal anti-*Mm*PCFT antibody. As shown in Fig. 5C, there was substantial expression of *Mm*PCFT protein in the duodenum and proximal jejunum localized exclusively to the apical brush-border membrane. The peptide antigen used to produce the anti-*Mm*PCFT antibody completely blocked staining of *Mm*PCFT, consistent with the high specificity of this antibody for *Mm*PCFT protein.

Alterations in MmPCFT mRNA levels in the proximal small intestine in response to dietary folate. A previous study (15) demonstrated that folate deprivation in mice resulted in increased levels of both FR-α and RFC mRNA. Using the RNA from these animals, we assessed the impact of folate deprivation on PCFT mRNA in the proximal small intestine in mice on a normal chow diet versus mice on a folate-deficient diet. As shown in Fig. 6, *inset*, *Mm*PCFT mRNA levels were increased in each of 10 folate-deficient mice compared with folate-replete mice (n = 7) without an overlap in levels between the two groups. Overall, the *Mm*PCFT mRNA level was increased by a factor of ∼13 in folate-deficient mice compared with folate-replete mice (Fig. 6).

DISCUSSION

The present study demonstrates that murine and rat PCFTs, like the human ortholog, are high-affinity carriers with a high degree of specificity for folates. Both *Mm*PCFT and *Rn*PCFT are highly specific for monoglutamate MTX but not polyglutamate derivatives of MTX. This explains, at the molecular level, why the transport of dietary folates across the luminal brush-border membranes of proximal small intestinal epithelial cells requires the hydrolysis of folate polyglutamates by γ-glutamyl carboxypeptidase II to monoglutamate forms before transport into enterocytes can occur (7).

Transport of folic acid, (6S)5-methylTHF, and MTX by mouse and rat PCFTs expressed in *Xenopus* oocytes was electrogenic, consistent with a net charge translocation during folate transport. The magnitude of the current was dependent on the extracellular folate concentration and on the extracellular pH. Alterations in protonation of the folate molecule do not occur over the pH range of 5.5 to 7.4 (20); however, at lower pHs, these measurements would be complicated by changes in
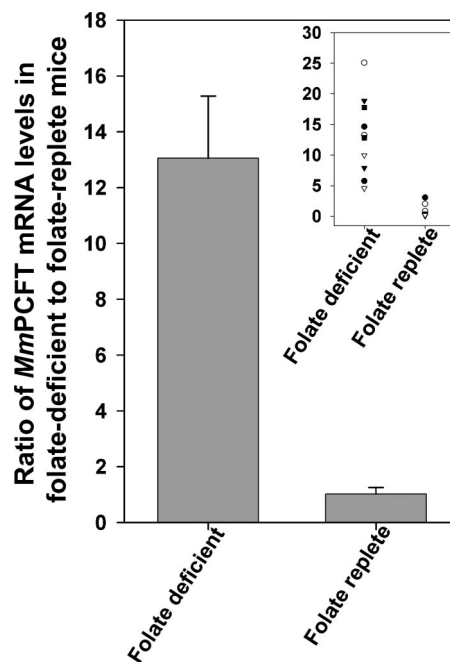

Fig. 6. *Mm*PCFT mRNA levels in the mouse proximal small intestine as a function of the dietary folate level. Mice were fed either a folate-replete or folate-deficient diet, after which PCFT levels in the proximal intestine were quantified by real-time RT-PCR. Data were normalized to GAPDH mRNA levels and presented as average fold changes relative to the average *Mm*PCFT level in mice fed a folate-replete diet (assigned a value of 1). *Inset*: *Mm*PCFT mRNA levels in individual mice from these two groups. Each symbol indicates an individual mouse. Data are means ± SE from 3 separate measurements.

substrate protonation, which, in turn, changes the concentration of the substrate recognized by the transporter. The change in current amplitude as a function of pH, under conditions in which changes in protonation of the folate molecule do not occur, suggest that pH changes not only alter the magnitude of the driving force for folate transport but may also titrate amino acids within PCFT that result in an alteration in the rate of transport. Studies are underway to identify the amino acids involved in these pH-dependent effects.

*Mm*PCFT has been previously reported to be a heme carrier protein (HCP1) that transports heme with low affinity (∼125 μM) and independent of pH (14, 25). Within the context of that report, HCP1 was predicted to consist of nine transmembrane domains with the NH2- and COOH-termini located intracellularly and extracellularly, respectively. However, the present study, along with the previous report from this laboratory, indicates that transport mediated by this carrier is highly specific and pH dependent for folates, with an affinity at least two orders of magnitude higher than that reported for hemin. These data, together with topological prediction based on multiple hydropathy analyses, also support intracellular localization of both the NH2- and COOH-termini of *Mm*PCFT and *Rn*PCFT expressed in HeLa cells and an even number of transmembrane segments, most likely 12. However, in view of the limitations of the methodologies employed, confirmation of the localization of the NH2- and COOH-termini and other elements of this transporter will require further verification of the secondary structure.

The functional properties of *Mm*PCFT and *Rn*PCFT are consistent with the folate transport activities that have been

reported for rat and mouse intestinal segments, brush-border membranes, and intestinal cell lines that have a low pH maximum (16, 29). Both transporters have a high level of folate transport activity at pH 6.0, the pH at the apical surface of the proximal small intestinal epithelium (17). *Mm*PCFT mRNA and protein were highly expressed in the duodenum and upper jejunum with the protein exclusively localized to the brush-border membrane, consistent with its functional role as the rate-limiting first step in the absorption of dietary folates. The functional role of *Mm*PCFT in intestinal folate absorption is further supported by the observation that *Mm*PCFT mRNA levels in the murine proximal small intestine increased 13-fold in mice fed a folate-deficient diet. It is of interest that both RFC and FR-α mRNA levels also increased in the same tissues from the same mice on a folate-deficient diet, indicating that expression of all these transporters is folate responsive (15). However, it is only PCFT that, in fact, mediates the translocation of folates at the acidic environment of the proximal small intestine at usual dietary folate levels. This conclusion is based on the observation that this gene is mutated in patients with hereditary folate malabsorption. Hence, this folate-responsive regulation of the *PCFT* gene is particularly important in folate deficiency states. It is possible, however, that some RFC-mediated transport can occur with the administration of pharmacological doses of folates, as in the treatment of hereditary folate malabsorption (6).

In addition to its high expression in the small intestine at the sites of folate absorption, PCFT is also highly expressed in other tissues. Very high expression of *Mm*PCFT mRNA was observed in the liver and kidney, tissues that manifest a high level of folate transport activity at low pH (1, 9). The major fraction of folates in the glomerular filtrate, which is at pH 6.8 (11), are reabsorbed at the proximal tubules. At this pH, PCFT has substantial folate transport activity, suggesting that it may play a direct role in reabsorption of folates at this site. This is supported by the presence of substantial low pH folate transport activity in brush-border membrane vesicles from the rat kidney (1). The contribution of PCFT to folate transport in the liver, where it is also highly expressed, is not clear. Transport of folates into the liver from the arterial system occurs at neutral pH; however, the pH within the hepatic portal sinusoids, where folates are delivered via the portal system from the intestine to hepatocytes, is not known and may be acidic (9). Data for human and rodent PCFTs indicate that there is residual 5-methylTHF transport activity at pH 7.0 so that this carrier can operate, albeit less efficiently, at neutral pH.

Beyond transport at the level of the cell membrane, PCFT may have other functions. For instance, this carrier may be incorporated into membrane vesicles that accommodate folate receptors and transport folates by receptor-mediated endocytosis or transcytosis (33). FR-α is highly expressed at the apical proximal renal tubule membrane and has been suggested to be a major route of folate reabsorption in the kidney (2). Folates bind to FRs that are anchored to the cell membrane via a glycosylphosphoinositol moiety. The resultant complex is internalized in a vesicle that traffics, intact, within the cytoplasm, where it is acidified, resulting in the release of the folate molecule from receptor (18, 19, 34). The mechanism by which folate is then exported from the vesicle has not been clarified. If PCFT is present in these endocytic vesicles, it could provide the route of folate transport into the cytoplasm using the

outward transvesicular proton gradient. Such a mechanism has been proposed earlier, although the identity of a vesicular transporter that could function at low pH is not known (12, 21). This mechanism could also explain, in part, why patients with hereditary folate malabsorption have a defect in folate transport into the central nervous system where the pH is neutral at the transport site but FR-α is highly expressed at the choroid plexus (32). The detection of substantial levels of PCFT mRNA in the mouse brain is consistent with this hypothesis.

Analysis of the NCBI GenBank genome database shows that PCFT is highly conserved in other mammalian species at the level of both the gene and primary protein structures, e.g., in the dog, rhesus monkey, and domestic cow and, to a lesser extent, in nonmammalian vertebrates such as birds, amphibians, and fish. Together with its functional conservation in humans, mice, and rats, this suggests that PCFT is evolutionarily conserved for intestinal folate absorption in mammalian species and likely plays this role in nonmammalian vertebrates as well. PCFT does not appear to be conserved in invertebrates according to a protein-protein BLAST search of the NCBI GenBank database using vertebrate PCFTs as queries, suggesting that this gene might have originated and evolved in vertebrates.

REFERENCES

1. **Bhandari SD, Joshi SK, McMartin KE.** Folate binding and transport by rat kidney brush-border membrane vesicles. *Biochim Biophys Acta* 937: 211–218, 1988.
2. **Birn H, Spiegelstein O, Christensen EI, Finnell RH.** Renal tubular reabsorption of folate mediated by folate binding protein 1. *J Am Soc Nephrol* 16: 608–615, 2005.
3. **Chattopadhyay S, Zhao R, Krupenko SA, Krupenko N, Goldman ID.** The inverse relationship between reduced folate carrier function and pemetrexed activity in a human colon cancer cell line. *Mol Cancer Ther* 5: 438–449, 2006.
4. **Chiao JH, Roy K, Tolner B, Yang CH, Sirotnak FM.** RFC-1 gene expression regulates folate absorption in mouse small intestine. *J Biol Chem* 272: 11165–11170, 1997.
5. **Fry DW, Yalowich JC, Goldman ID.** Rapid formation of poly-gamma-glutamyl derivatives of methotrexate and their association with dihydrofolate reductase as assessed by high pressure liquid chromatography in the Ehrlich ascited tumor cell in vitro. *J Biol Chem* 257: 1890–1896, 1982.
6. **Geller J, Kronn D, Jayabose S, Sandoval C.** Hereditary folate malabsorption: family report and review of the literature. *Medicine (Baltimore)* 81: 51–68, 2002.
7. **Halsted CH, Ling EH, Luthi-Carter R, Villanueva JA, Gardner JM, Coyle JT.** Folylpoly-gamma-glutamate carboxypeptidase from pig jejunum. Molecular characterization and relation to glutamate carboxypeptidase II. *J Biol Chem* 273: 20417–20424, 1998.
8. **Henderson GB, Strauss BP.** Characteristics of a novel transport system for folate compounds in wild-type and methotrexate-resistant L1210 cells. *Cancer Res* 50: 1709–1714, 1990.
9. **Horne DW.** Transport of folates and antifolates in liver. *Proc Soc Exp Biol Med* 202: 385–391, 1993.
10. **Jansen M, Akabas MH.** State-dependent cross-linking of the M2 and M3 segments: functional basis for the alignment of GABAA and acetylcholine receptor M3 segments. *J Neurosci* 26: 4492–4499, 2006.
11. **Jaramillo-Juarez F, Aires MM, Malnic G.** Urinary and proximal tubule acidification during reduction of renal blood flow in the rat. *J Physiol* 421: 475–483, 1990.
12. **Kamen BA, Smith AK, Anderson RGW.** The folate receptor works in tandem with a probenecid-sensitive carrier in MA104 cells in vitro. *J Clin Invest* 87: 1442–1449, 1991.

13. **Lassmann T, Sonnhammer EL.** Kalign, Kalignvu and Mumsa: web servers for multiple sequence alignment. *Nucleic Acids Res* 34: W596–W599, 2006.

14. **Latunde-Dada GO, Takeuchi K, Simpson RJ, McKie AT.** Haem carrier protein 1 (HCP1): expression and functional studies in cultured cells. *FEBS Lett* 580: 6865–6870, 2006.

15. **Liu M, Ge Y, Cabelof DC, Aboukameel A, Heydari AR, Mohammad R, Matherly LH.** Structure and regulation of the murine reduced folate carrier gene: identification of four noncoding exons and promoters and regulation by dietary folates. *J Biol Chem* 280: 5588–5597, 2005.

16. **Mason JB, Rosenberg IH.** Intestinal absorption of folate. In: *Physiology of the Gastrointestinal Tract*, edited by Johnson LR. New York: Raven, 1994, p. 1979–1995.

17. **McEwan GT, Daniel H, Fett C, Burgess MN, Lucas ML.** The effect of *Escherichia coli* STa enterotoxin and other secretagogues on mucosal surface pH of rat small intestine in vivo. *Proc R Soc Lond B Biol Sci* 234: 219–237, 1988.

18. **Murphy RF, Powers S, Cantor CR.** Endosome pH measured in single cells by dual fluorescence flow cytometry: rapid acidification of insulin to pH 6. *J Cell Biol* 98: 1757–1762, 1984.

19. **Paulos CM, Reddy JA, Leamon CP, Turk MJ, Low PS.** Ligand binding and kinetics of folate receptor recycling in vivo: impact on receptor-mediated drug delivery. *Mol Pharmacol* 66: 1406–1414, 2004.

20. **Poe M.** Acidic dissociation constants of folic acid, dihydrofolic acid, and methotrexate. *J Biol Chem* 252: 3724–3728, 1977.

21. **Prasad PD, Mahesh VB, Leibach FH, Ganapathy V.** Functional coupling between a bafilomycin A_1-sensitive proton pump and a probenecid-sensitive folate transporter in human placental choriocarcinoma cells. *Biochim Biophys Acta Mol Cell Res* 1222: 309–314, 1994.

22. **Qiu A, Jansen M, Sakaris A, Min SH, Chattopadhyay S, Tsai E, Sandoval C, Zhao R, Akabas MH, Goldman ID.** Identification of an intestinal folate transporter and the molecular basis for hereditary folate malabsorption. *Cell* 127: 917–928, 2006.

23. **Said HM.** Recent advances in carrier-mediated intestinal absorption of water-soluble vitamins. *Annu Rev Physiol* 66: 419–446, 2004.

24. **Sharif KA, Goldman ID.** Rapid determination of membrane transport parameters in adherent cells. *Biotechniques* 28: 926–928, 930, and 932, 2000.

25. **Shayeghi M, Latunde-Dada GO, Oakhill JS, Laftah AH, Takeuchi K, Halliday N, Khan Y, Warley A, McCann FE, Hider RC, Frazer DM, Anderson GJ, Vulpe CD, Simpson RJ, McKie AT.** Identification of an intestinal heme transporter. *Cell* 122: 789–801, 2005.

26. **Sierra EE, Goldman ID.** Characterization of folate transport mediated by a low pH route in mouse L1210 leukemia cells with defective reduced folate carrier function. *Biochem Pharmacol* 55: 1505–1512, 1998.

27. **Smith SB, Kekuda R, Gu X, Chancy C, Conway SJ, Ganapathy V.** Expression of folate receptor alpha in the mammalian retinol pigmented epithelium and retina. *Invest Ophthalmol Vis Sci* 40: 840–848, 1999.

28. **Stover PJ.** Physiology of folate and vitamin B12 in health and disease. *Nutr Rev* 62: S3–S12, 2004.

29. **Wang Y, Rajgopal A, Goldman ID, Zhao R.** Preservation of folate transport activity with a low-pH optimum in rat IEC-6 intestinal epithelial cell lines that lack reduced folate carrier function. *Am J Physiol Cell Physiol* 288: C65–C71, 2005.

30. **Wang Y, Zhao R, Goldman ID.** Characterization of a folate transporter in HeLa cells with a low pH optimum and high affinity for pemetrexed distinct from the reduced folate carrier. *Clin Cancer Res* 10: 6256–6264, 2004.

31. **Wang Y, Zhao R, Russell RG, Goldman ID.** Localization of the murine reduced folate carrier as assessed by immunohistochemical analysis. *Biochim Biophys Acta* 1513: 49–54, 2001.

32. **Weitman SD, Weinberg AG, Coney LR, Zurawski VR Jr, Jennings DS, Kamen BA.** Cellular localization of the folate receptor: potential role in drug toxicity and folate homeostasis. *Cancer Res* 52: 6708–6711, 1992.

33. **Williams WM, Huang KC.** Renal tubular transport of folic acid and methotrexate in the monkey. *Am J Physiol Renal Fluid Electrolyte Physiol* 242: F484–F490, 1982.

34. **Yang J, Chen H, Vlahov IR, Cheng JX, Low PS.** Characterization of the pH of folate receptor-containing endosomes and the rate of hydrolysis of internalized acid-labile folate-drug conjugates. *J Pharmacol Exp Ther* 321: 462–468, 2007.

35. **Zhao R, Gao F, Hanscom M, Goldman ID.** A prominent low-pH methotrexate transport activity in human solid tumor cells: Contribution to the preservation of methotrexate pharmacological activity in HeLa cells lacking the reduced folate carrier. *Clin Cancer Res* 10: 718–727, 2004.

36. **Zhao R, Hanscom M, Goldman ID.** The relationship between folate transport activity at low pH and reduced folate carrier function in human Huh7 hepatoma cells. *Biochim Biophys Acta* 1715: 57–64, 2005.

37. **Zhao R, Min SH, Qiu A, Sakaris A, Goldberg GL, Sandoval C, Malatack JJ, Rosenblatt DS, Goldman ID.** The spectrum of mutations in the PCFT gene, coding for an intestinal folate transporter, that are the basis for hereditary folate malabsorption. *Blood* 110: 1147–1152, 2007.